Characterizing the critical challenges of Li-metal solid-state batteries: From micrometer to centimeter

So-Yeon Ham, Ashley Cronk, Ying Shirley Meng,* and Jihyun Jang*

Lithium-metal solid-state batteries (LiMSSBs) are potentially one of the most promising next-generation battery technologies that can enable high energy density without compromising safety. However, their implementation on a practical level has yet to be demonstrated due to the incompatibility of solid-state components, electro-chemo-mechanical interfacial degradation, and ultimately, dendrite formation which limits practical operation. In this article, we systematically address the key challenges at various length scales from interfacial issues at the material level to system-level challenges at the more practical cell level, where characterization tools and methodologies are presented to shed light on the main degradation mechanisms. A full suite of tools ranging from electrochemical and chemical analysis to microscopy are recommended with the limitations and capabilities of each discussed. Finally, an outlook on how these techniques can accelerate the further development of next-generation LiMSSBs is discussed.

Introduction

Lithium-metal solid-state batteries (LiMSSBs) are currently one of the most promising next-generation energy-storage strategies to enable high energy–density batteries while combating the safety challenges associated with Li metal and liquid electrolytes. As the prevalence of electric vehicles (EVs) increases, the demand for better performance such as longer range and faster charging times is required to make EVs more desirable than their fossil fuel counterparts.[1] Currently, state-of-the-art lithium-ion batteries have limited energy and power density originating from the use of liquid electrolyte and graphite anodes, which possess limited specific capacity (372 mAh g^{-1}) and lithiation rates.[2] Moreover, the thermal runaway issue coming from the flammable conventional organic liquid electrolyte can be mitigated by changing to nonflammable solid-state electrolytes (SSEs).[3–7] In addition, all-solid-state batteries utilizing lithium-metal anodes can possibly deliver gravimetric and volumetric energy densities up to 400 Wh kg^{-1} and 900 Wh L^{-1}, respectively,[8] which can deliver longer ranges and enable currently unattainable electrified applications such as electrified aircraft. The increase in energy density is due to lithium metal's high specific capacity (3860 mAh g^{-1}) and the lowest reaction voltage (−3.04 V versus NHE). It also has the potential compatibility with stable SSE to combat interphase growth and mass transfer limitations present within lithium-metal liquid systems.[9,10] However, in practice, the implementation of lithium metal within solid-state batteries has presented multiscale obstacles (**Figure 1**), from interface to full cell and practical level. There are numerous interfaces between each component of LiMSSBs, such as cathode composite and catholyte SSE, lithium metal and SSE, and the SSE layer itself. These interfaces can be subjected to chemical and electrochemical instability[11,12] leading to irreversible lithium loss, large resistance growth, and chemo-mechanical degradation of SSE films. It will eventually cause low usable current densities, limiting charge/discharge rates, and power densities for practical applications as well as dendritic growth. At the full-cell level, accumulated interface level challenges and larger scale volume change originating from the imbalance of cathode/anode expansion/shrinkage during the cycling[13,14] create the pores and dead region where it cannot participate in the reaction, which leads to nonuniform current and thus

So-Yeon Ham, Materials Science and Engineering Program, University of California, San Diego, La Jolla, USA; soham@ucsd.edu
Ashley Cronk, Materials Science and Engineering Program, University of California, San Diego, La Jolla, USA; acronk@ucsd.edu
Ying Shirley Meng, Department of NanoEngineering, University of California, San Diego, La Jolla, CA, USA; Pritzker School of Molecular Engineering, The University of Chicago, Chicago, USA; shirleymeng@uchicago.edu
Jihyun Jang, Department of Chemistry, Sogang University, Seoul, Republic of Korea; jihyunjang@sogang.ac.kr
*Corresponding author
So-Yeon Ham and Ashley Cronk are co-first authors and have contributed equally to the work.
doi:10.1557/s43577-023-00630-4

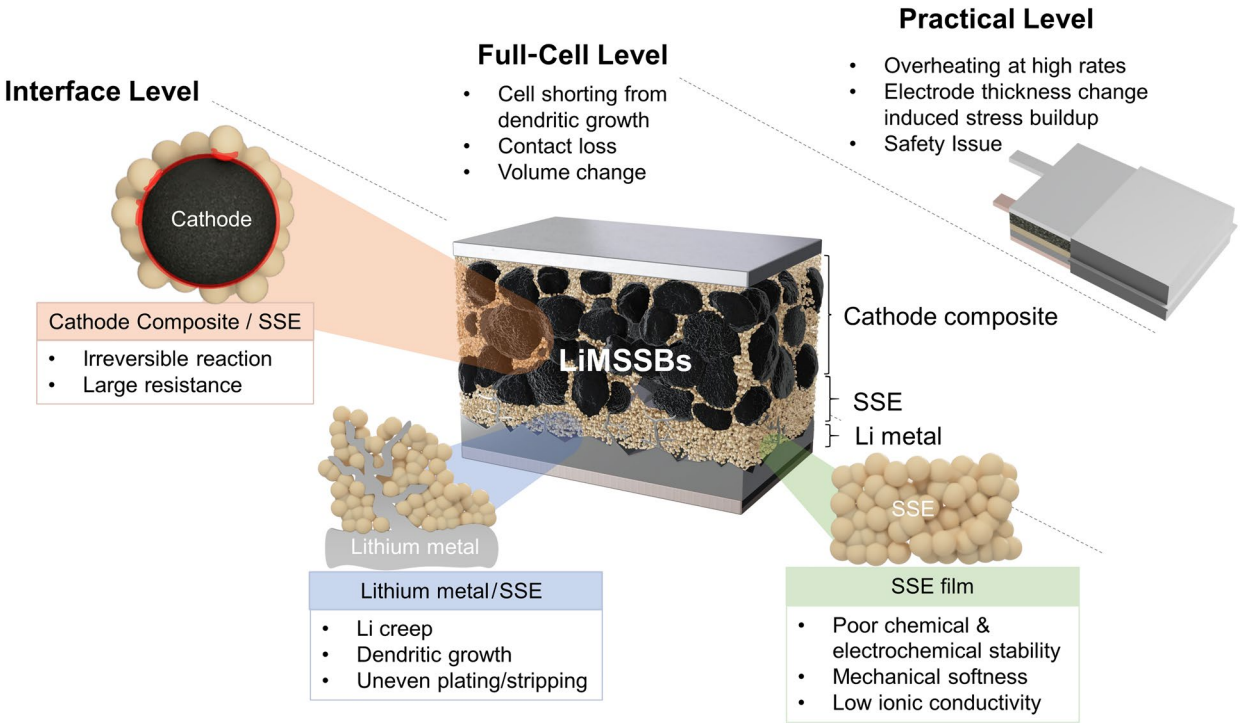

Figure 1. Schematics of the list of multiscale challenges for lithium-metal solid-state batteries (LiMSSBs) to overcome from interface molecular level to practical cell level. SSE, solid-state electrolyte.

dendritic lithium-metal growth, which can generate the short-circuit behavior. Further, transitioning from laboratory-scale pellet-type full cells to larger form factors such as pouch cells requires careful consideration in material selection and compatibility as chemo-mechanical degradation from anode and cathode volume change in addition to interfacial instability are exacerbated as areal capacity increases. All of these combined problems at various length scales contribute to the cell failure of LiMSSBs. Without deconvoluting individual factors of cell degradation by identifying the root cause, the realization of LiMSSBs is questionable. Therefore, characterization strategies are imperative to diagnose cell failure and facilitate the development of analysis methods to aid in the material selection, design, and improvement of all-solid-state lithium-metal batteries.

Issues for lithium-metal solid-state batteries

One of the limiting factors of solid-state versus conventional liquid is lithium-ion transport within the electrodes. Liquid electrolytes can easily percolate through porous electrodes whereas in solid-state, lithium-ion transport is limited by solid–solid diffusion. An ideal SSE would exhibit high bulk ionic conductivity and low electronic conductivity, while also maintaining good contact and deformability with the active materials and cathode/anode interfaces. With the discovery of $Li_{10}GeP_2S_{12}$ (LGPS), a superionic electrolyte with ionic conductivity competitive with conventional liquid electrolytes at room temperature (12 mS cm^{-1}),[15] interest in SSE development surged. Other SSE candidates such as Li_2S-P_2S_5 sulfide ceramic glasses were also reported with ionic conductivity higher than liquid electrolytes of up to 17 mS cm^{-1}.[16] Despite the advances in SSE development from an ion conduction perspective, other materials properties should be considered critically for the performance such as interfacial stability. For instance, despite their high ionic conductivity, sulfide-based SSEs demonstrate narrow electrochemical windows; nonetheless, the reduced degradation products exhibit desirable properties that allow lithium passivation at lower potentials.[12,14,17] This makes sulfide-based SSEs a usual choice as an anolyte or as a separator layer within the solid-state system. In order to be implemented within the cathode composite, coating cathode active materials with electronically insulating and lithium-ionically conducting layers is one widely used strategy to minimize interfacial degradation.[18–20] The use of more stable SSEs such as chlorides and oxides is another strategy to minimize interfacial degradation at the cathode potentials, but usually at the cost of ionic conductivity[21,22] or deformability.[23] Therefore, in addition to SSE selection, methodologies to analyze the (electro)chemical stability at the cathode or anode interface are necessary to develop better solid-state batteries.

The mechanical property of lithium is one of the most important aspects to consider when building LiMSSBs. This is because the reported yield strength values of polycrystalline lithium metal in micrometer-sized dimensions are below 1 MPa in compression mode,[24] which is smaller pressure than common

cycling conditions of solid-state cells. With this in mind, the most important mechanical property of lithium metal in a solid-state battery setup would be the continual deformation under persistent compression loads, which is called "creep." Creep plays a crucial role when forming intimate contact between lithium and the SSE layer, affecting the critical current density. The creep rate is dependent on several factors such as applied pressure, temperature, and lithium thickness.[25] The study examining all these factors on lithium foil showed that applied pressure of less than 2 MPa was enough to induce significant creep deformation for all samples. On the other hand, an appropriate creep rate could facilitate better contact between lithium metal and adjacent layers. In fact, some studies reported that the stack pressure of solid-state batteries induced creep contributions to a higher fraction of contact between lithium metal and SSE both in the computational model[26] and in the experiment.[27] However, recent research on Li metal showed that Li metal with submicron size could support more than 200 MPa, indicating there is a clear difference in yield strength between bulk Li metal and nanometer-scale Li whisker.[28] The result implies the mechanical properties of bulk Li on the anode side and dendritic Li within SSE should be carefully considered when designing LiMSSBs.[29] Also, the mechanical properties of SSE itself are another important factor to consider, because the densification of the SSE layer also contributes to the critical current densities, where pores and grain boundaries of SSE could act as preferable sites for lithium dendrite growth.[30] The complexity of the plastic deformation of Li and grain boundaries and pores of the SSE layer all contribute to dendrite propagation leading to the cell shorting. Accordingly, examining the mechanical properties and degradation of lithium and SSE is vital to understanding the performances and degradations of LiMSSBs.

Low critical current density (CCD) is a widely accepted problem of LiMSSBs. The CCD is often defined as the current density at which lithium dendrite penetrates the SSE separator and makes the cell fail by short-circuiting. The reported room-temperature CCD of LiMSSBs is limited to 1 mA cm^{-2}, which is way lower than a commercial requirement. The reported CCD values in literature widely vary because CCD is dependent on various factors such as cell stack pressure, plating capacity, cell component chemistry, and areal capacity. The mechanism of dendritic lithium growth is still under study, but it is closely related to Li/SSE interfacial void formation, which leads to subsequent porosity, surface roughness, and contact loss. There are many reports showing lithium dendrites nucleate at interfacial voids and cracks at the lithium-metal and SSE interfaces. The interfacial void formation originates from the imbalance between lithium-ion fluxes at the Li/SSE interface. In the LiMSSB cycling condition with certain stack pressure, there are three lithium-ion fluxes involved: (1) $J_{Lithium\text{-}ion\ migration}$: lithium-ion migration driven from applied current, (2) $J_{Lithium\text{-}ion\ diffusion}$: self-diffusion of lithium atoms driven by the concentration gradient, and (3) $J_{Lithium\ creep}$: lithium creep driven by the stack pressure. To suppress the void formation and subsequent lithium dendrite growth, maintaining the balance is crucial.[31] Therefore, the research discussed in this article will cover the various tools to observe the dendritic lithium growth and also the *operando* characterization to capture the void or dendrite formation.

Interface-level (micrometer-level) characterization

Beyond ionic conductivity, the stability of the SSE at the anode or cathode interface, within the cathode composite, and the separator layer itself is crucial for realizing highly energy-dense solid-state batteries. In an ideal case, the SSE should exhibit good stability at both electrodes, facilitating lithium transport as the cell is cycled. If the SSE is not (electro)chemically stable, degradation products can be formed either from chemical or electrochemical reactions. These formed products can potentially be detrimental to the entire system, creating growing interphase layers that could be insulative and hinder lithium transport. To evaluate the (electro)chemical stability, electrochemical techniques like linear sweep voltammetry and cyclic voltammetry are typically employed to extract the electrochemical stability window as done in prior work.[17,32–34] In these works, cell setup and electrode configurations are critical in order to obtain accurate results (**Figure 2**). Han et al. highlight the importance of mixing the SSE with high-surface-area conductive material within the composite electrode in order to facilitate sufficient interfacial reactions and accurately obtain electrochemical stability windows of LGPS and $Li_7La_3Zr_2O_{12}$ (LLZO) SSEs, expanding on previous stability results (Figure 2a–b).[33] Electrochemical stability and redox activity of argyrodite Li_6PS_5Cl (LPSCl) and garnet LLZO were also investigated by Schwietert et al.,[32] where constant current charge and discharge were used to perform differential capacity analysis (Figure 2c). These results coupled with ^{31}P NMR and first-principles calculations were used to further identify redox species after (de)lithiation, where their electrochemical stability was determined by the oxidation and reduction potentials of S and P for LPSCl and O and Zr for LLZO. Some SSEs exhibit reversible or irreversible behavior, depending on the operating voltage and the resulting decomposition products that are formed. The reversibility of LPSCl was also studied by Tan et al., where ^{31}P and ^{7}Li NMR coupled with x-ray photoelectron spectroscopy (XPS) was employed to confirm decomposition products at certain cutoff potentials.[17] The relationship between electrochemical stability windows and resulting decomposition products are a significant factor that affects the overall performance of LiMSSBs.

The (electro)chemical stability of SSEs determines the interfacial reactions that occur at the cathode and anode potentials. Electrochemical impedance spectroscopy (EIS) can be used to study the impedance of interfacial layers formed at the surface between SSE and active materials, and allow the characterization of the solid-electrolyte interface (SEI) or cathode–electrolyte interface (CEI). Typically, EIS is used to study the resistance of a system or resulting ionic conductivities of SSEs as shown in Figure 2d, for example, Bron et al.

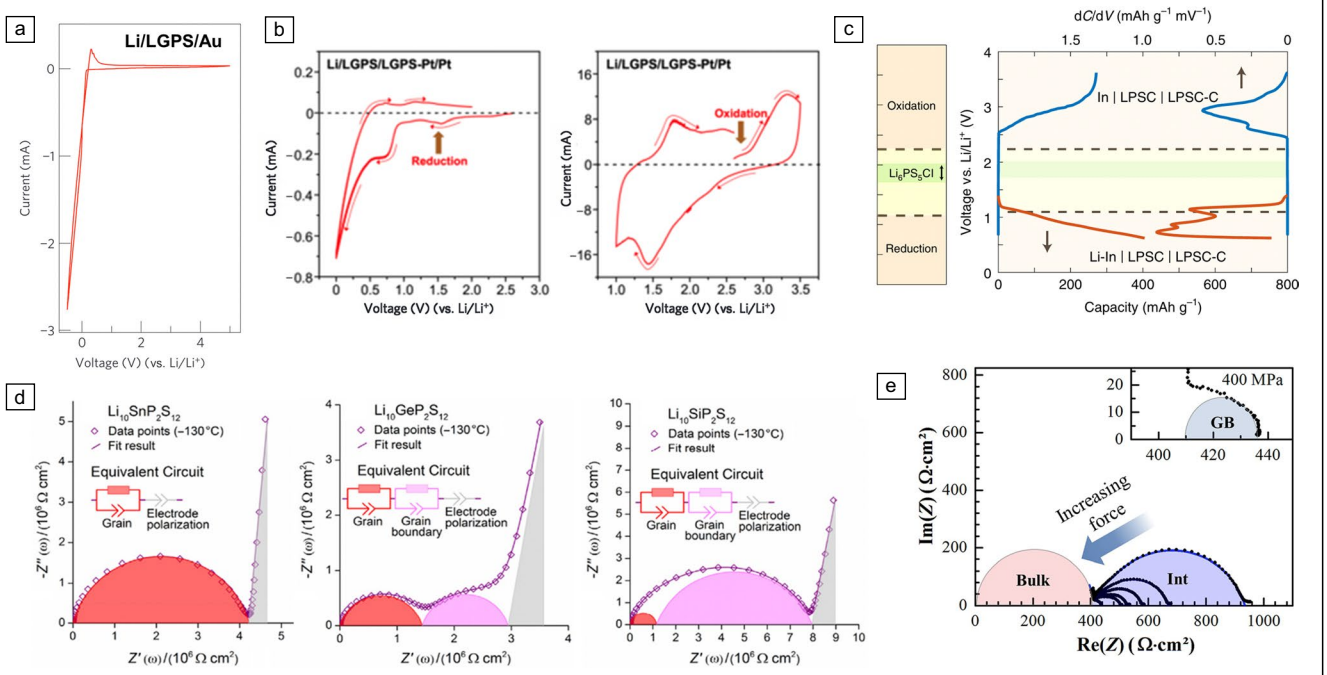

Figure 2. (a) Cyclic voltammetry of LGPS using Li/LGPS/Au cell configuration. Reprinted with permission from Reference 15. © 2021 Nature Publishing Group. (b) Cyclic voltammetry scans of LGPS using Li/LGPS/LGPS-Pt/Pt cell configuration showing the difference in obtained electrochemical stability depending on cell setup. Reprinted with permission from Reference 33. © 2016 Wiley-VCH. (c) Constant current charge and discharge and dQ/dV of Li-In/LPSCl/carbon cells. Reprinted with permission from Reference 32. © 2020 Nature Publishing Group. (d) Nyquist plots of doped LGPS electrolytes with various dopants Sn and Si showing respective impedance contributions. Reprinted with permission from Reference 35. © 2016 Elsevier. (e) Nyquist plots of LLZO electrolyte showing the interfacial resistance reduction with increased compressive force. Reprinted with permission from Reference 36. © 2019 American Chemical Society. GB, grain boundary.

used equivalent circuit fitting results to deconvolute impedance contributions from doping LGPS with low-cost elements such as Al, Sn, and Si.[35] EIS was also employed to study the pressure-dependent SEI resistance of garnet LLZO electrolytes when in contact with lithium metal (Figure 2e), where Krauskopf et al. reported negligible interfacial resistance (0 Ω cm^{-2}) when LLZO was pressed at 100 MPa, owing these results to good contact geometry where the interface remains morphologically stable at current densities of 100 μA cm^{-2}.[36]

Beyond indirect tools such as impedance quantification, direct evidence such as visualizing SEI growth is a powerful tool that allows the direct observation of interfacial layers, decomposition products, and lithium dendritic growth. Wang et al. used a combination of EIS with time-of-flight secondary ion mass spectrometry (ToF–SIMS) high-resolution imaging and depth profiling of the $Li_{1.15}Y_{0.15}Zr_{1.85}(PO_4)_3$ (LYZP) electrolyte to relatively quantify the interfacial species after contact with lithium metal and studied their distribution. This work demonstrated that even highly stable SSEs can still promote dendritic growth, for this case, LYZP reduced to form high electronic conductivity metallic Zr, and its distribution was mapped in 3D (**Figure** 3a).[11] *Operando* analysis is another tool to investigate the interfacial dynamics in real time. Davis et al. used *operando* XPS and video microscopy to investigate the interfacial decomposition of LGPS and LPSCl in anode-free cells, studying the difference in degradation properties and how it either facilitates interfacial growth or stabilizes (Figure 3b). As lithium was plated on the LPSCl, the growth of Li_xP and Li_3P was confirmed, which eventually stabilized. For the LGPS case, in addition to Li_xP, Li_3P, metallic Ge was also detected, which is electrically conducting and continually consumes lithium.[37] This work shed light on SSE selection for anode-free configurations and how degradation products influence battery performance.

In addition to studying the anode interface, SSE compatibility with the cathode interface is also important. Jang et al. developed a methodology to use EIS in order to study the chemical compatibility of LPSCl with the high-voltage $LiNi_{0.5}Mn_{1.5}O_4$ (LNMO) cathode material, where an interlayer was formed even before cycling (Figure 3c). In that work, SSE selection in addition to cathode coatings to mitigate CEI growth was highlighted, enabling the improved performance of the LNMO cathode within the all-solid-state system.[38] Interfacial stability of the CEI can also be investigated using XPS, which allows the local determination of chemical species at the surface. Auvergniot et al. compared the performance of the sulfide-based LPSCl electrolyte with $LiNi_{1/3}Mn_{1/3}Co_{1/3}O_2$ (NMC111), $LiMn_2O_4$ (LMO), and $LiCoO_2$ (LCO) cathodes (Figure 3d). It was observed that the LMO cathode exhibited the worst cycling performance versus NMC and LCO when paired with LPSCl. XPS results from the S 2*p* and P 2*p* spectra showed clear signs of decomposition of the LMO-LPSCl

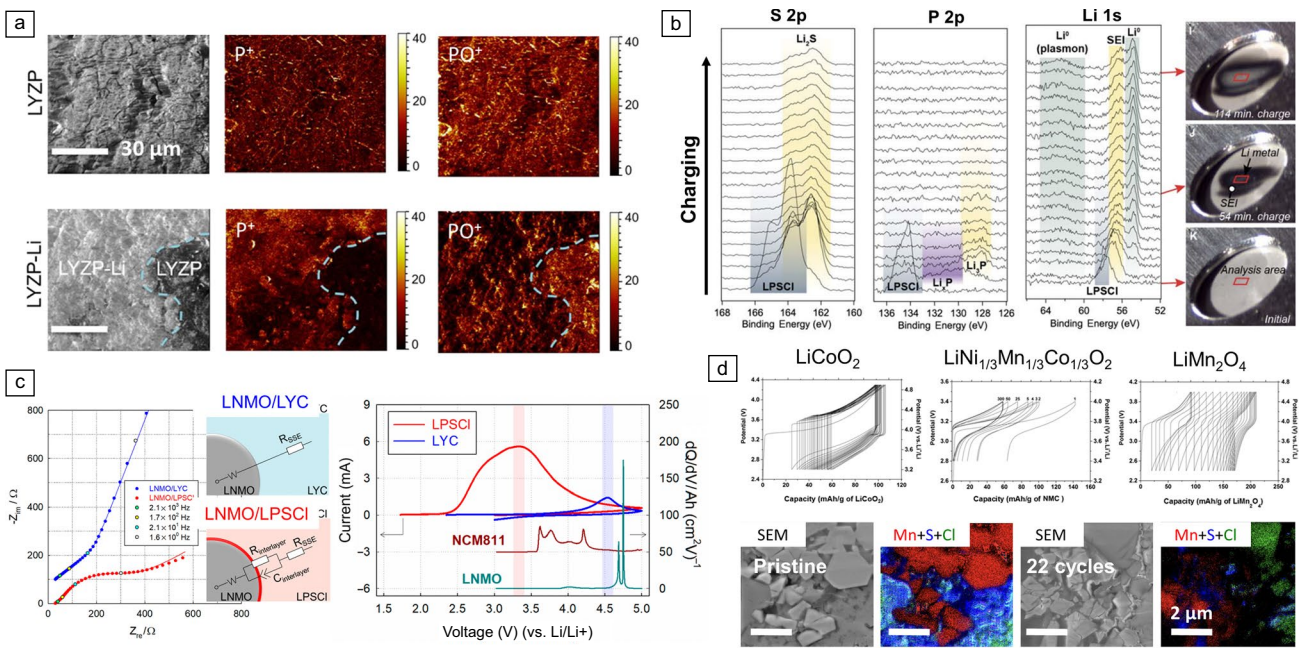

Figure 3. (a) Time-of-flight–secondary ion mass spectrometry mapping of LYZP and LYZP-Li. Reprinted with permission from Reference 11. © 2018 American Chemical Society. (b) (Left) *Operando* x-ray photoelectron spectroscopy of LPSCl and lithium metal at different states of charge. (Right) Corresponding optical images of the cell. Reprinted with permission from Reference 37. © 2021 The Electrochemical Society. (c) (Left) Nyquist plot from electrical impedance spectroscopy measurement and the equivalent circuit. (Right) Cyclic voltammetry curves of LPSCl/C (red) and LYC/C (blue) composites all-solid-state half-cells and the first cycle dQ/dV plots of two cathodes (NCM811 and LNMO) half-cells in the liquid electrolyte. Reprinted with permission from Reference 38. © 2022 American Chemical Society. (d) (Top) Voltage profiles of LCO, NMC111, and LMO using LPSCl electrolyte. (Bottom) Scanning electron microscopy (SEM) images of LMO cathode in a pristine state and after 22 cycles showing LPSCl decomposition. Reprinted with permission from Reference 39. © 2017 American Chemical Society.

system even in the pristine state, reinforcing the chemical incompatibility and reactivity of LPSCl at the LMO surface. XPS and SEM confirmed the decomposition of LPSCl into elemental sulfur, polysulfides, P_2S_x species, and phosphates.[39] These decomposition results were further supported by Cronk et al., where degradation of LPSCl at the carbon-coated $LiFePO_4$ (LFP) interface was ascribed to its poor performance and lack of studies within inorganic all-solid-state batteries. XPS, EIS, XRD, and Raman spectroscopy were used to confirm the formation of insulative decomposition products, while the use of a more stable SSE such as Li_2ZrCl_6 (LZC) was employed to mitigate CEI growth and enable high rate and long cycling of LFP in all-solid-state batteries.[34]

In addition to ionic conductivity and (electro)chemical stability, the mechanical properties of SSEs are another important feature of LiMSSBs. This is because good interfacial contact is required between cathode active materials, SSEs, and anodes to facilitate uniform current density and lithium diffusion between all layers. Therefore, easily deformable, mechanically compliant SSEs are desirable for not only fabrication ease, but also to accommodate volume change within the cathode composite or at the anode interface. Previous reports found that higher shear modulus prevents dendrite formation and ductile SSEs better accommodate stress–strain.[40] However, characterizing the mechanical properties of SSEs can be challenging due to their instability in ambient conditions requiring air-tight measurements. Atomic force microscopy and indentation are a popular method to determine the local mechanical properties of materials, including hardness, and has been evaluated in prior work.[41] Due to the air-tight requirements of SSEs, these techniques are usually done in the glove box. One nondestructive method is the ultrasonic pulse method, which is a technique that enables the determination of shear modulus, Poisson's ratio, elastic modulus, and bulk modulus by measuring the time it takes for vibrational energy to travel through a medium, measuring the velocity. Sakuda et al. employed the ultrasonic pulse method to study the elastic modulus of the garnet-type LLZO and sulfide glasses ($75Li_2S{\cdot}25P_2S_5$).[42] Their work confirmed the high elastic modulus of oxide electrolytes and why sintering is usually required to create densified oxide pellets. In addition, they found that the Li_2S content heavily influenced the elastic modulus, where a higher molar content increased the SSE stiffness. It was also found that doping the sulfide glasses with lithium halides reduced the elastic modulus, facilitating more deformable electrolytes.[43] That being said, densification can also be evaluated using a scanning electron microscope-focused ion beam (SEM–FIB), where SSE is compacted under fabrication pressures and milled to determine the porosity. This method was used by Cronk et al., where cross-sectional SEM–FIB validated the hypothesis that halide SSEs exhibit less porosity and more intimate contact.[34]

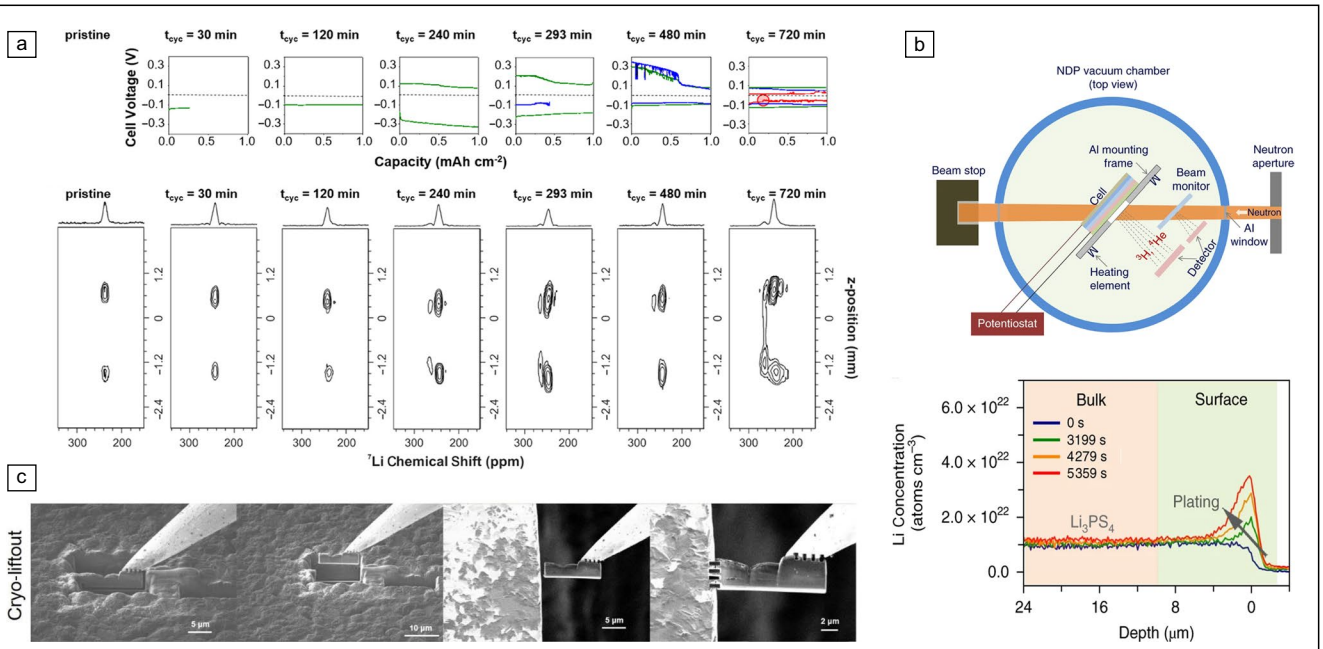

Figure 4. (a) The constant current plating and stripping (top) correlated with the ^{7}Li NMR CSI (bottom), which shows the lithium dendritic growth. Reprinted with permission from Reference 44. © 2019 American Chemical Society. (b) The experimental setup of neutron depth profiling (NDP) for probing lithium in the solid-electrolyte layer (top) and lithium concentration from the depth profiling (bottom). Reprinted with permission from Reference 45. © 2019 Nature Publishing Group. (c) The demonstration of cryo-liftout for lithium-metal electrode and LiPON interface. Reprinted with permission from Reference 48. © 2020 Cell Press.

Cell-level (millimeter-level) characterization

For lithium dendrite growth being the detrimental part of LiMSSBs, characterizing lithium dendrite has been extensively studied with various equipment. However, because the initiation and propagation of dendrite are buried in the SSE layer, the characterization should be conducted in a way that involves either sensing lithium dendrite in a nondestructive way or cutting the cell to expose the dendrite. Marbella et al. used ^{7}Li nuclear magnetic resonance (NMR) chemical shift imaging (CSI) to probe lithium microstructure changes and chemical information.[44] **Figure** 4a shows the cell data from constant current plating and stripping at the same current density of 0.5 mA cm^{-2} and stopped at different times. By correlating top cell voltage data and bottom ^{7}Li CSI data, the evolution of lithium dendrite growth and its microstructural change was observed without damaging the cell. Neutron depth profiling (NDP) is another nondestructive tool to investigate the lithium concentration in solid-electrolyte separators. Han et al. performed NDP on solid-state batteries with three different SSEs and monitored the dynamic evolution of lithium profiles.[45] SSEs with a relatively higher electronic conductivity such as LLZO and Li_3PS_4 showed an increase in lithium concentration with longer plating of lithium (Figure 4b). This higher lithium NDP count increased with higher temperatures due to the higher electronic conductivity at elevated temperatures. This study showed that electronic conductivity also plays a crucial role in regulating dendrite growth in solid-state batteries, thus when selecting the SSE, not only the lithium-ion ionic conductivity, but also the electronic conductivity of SSE itself, should be a crucial parameter to take into consideration. Because the buried interface hinders the observation of dendrite growth, the direct morphological observation of lithium dendrite of contact loss requires the cross-sectional cut using FIB. There are various kinds of ion beam sources for FIB; Ga^{+} is a more conventional source and the plasma such as Xe^{+} or Ar^{+} are emerging sources for their higher milling rate and less redeposition with certain materials.[46] Lu et al. used the plasma-FIB to cut the whole lithium-metal layer and observe the Li/LPS interface.[47] The study showed the evolution of contact loss with stripping capacity accumulation, which will lead to uneven plating of lithium for the next cycle and eventually become dendrite. The Ga^{+} source also could be used in investigating lithium-metal interphase in a cryo-environment to minimize the beam-induced damage as Cheng et al. did in the cryogenic transmission electron microscopy study of the Li/lithium phosphorus oxynitride (LiPON).[48] In the study, the cryo-Ga^{+} FIB milling was performed to preserve the Li/LiPON interphase, and the liftout process was also demonstrated in the cryo-environment utilizing the redeposition as the connecting agent between the lamella and the liftout probe (Figure 4c).

The *operando* study of LiMSSB shed light on a better understanding of how the cell actually operates, correlating the electrochemical data to chemical and morphological characterization. X-ray tomography (XTM) is useful in a way that it is nondestructive and can be measured *in situ* or *operando* to provide porosity, surface area, tortuosity, and volume change with the appropriate cell design.[49] However, the contrast in the images is dominated by the x-ray attenuation coefficient

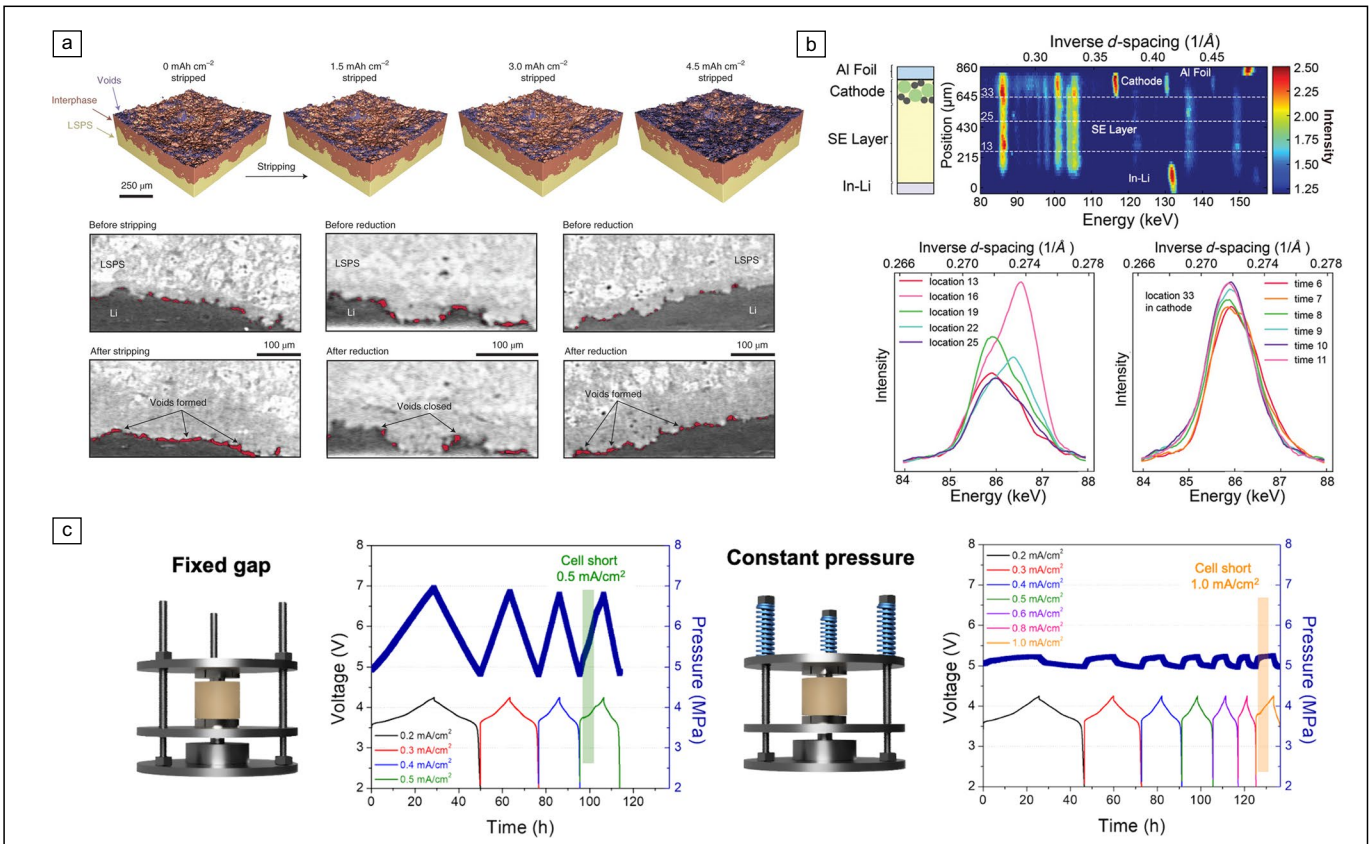

Figure 5. (a) Three-dimensional reconstructed and segmented scans of Li/LSPS interphase (top) and 2D x-ray images showing the contact loss. Reprinted with permission from Reference 51. © 2023 Nature Publishing Group. (b) The diffraction contour plot using energy-dispersive x-ray diffraction of LiMSSB (top) and the x-ray diffraction spectra of specific energy range as a function of spatial position (bottom left) and time (bottom right). Reprinted with permission from Reference 52. © 2021 Wiley-VCH. (c) The *operando* electrochemical pressiometric measurement for the fixed gap (left) and the constant pressure setup (right). Reprinted with permission from Reference 27. © 2023 Elsevier. SE, solid-electrolyte.

of each material,[50] missing chemical information. There have been many studies that applied XTM to battery research, especially synchrotron radiation *operando* x-ray tomographic microscopy (SRXTM) could be used to directly observe the nanometer- to micrometer-level reaction. Lewis et al. performed operando SRXTM to investigate the interphase evolution during the plating and stripping of lithium metal in Li/$Li_{10}SnP_2S_{12}$ (LSPS)/Li solid-state cell.[51] The 3D reconstructed and segmented renderings are shown in **Figure** 5a, showing the voids were formed to induce contact loss as more lithium was stripped. The 2D x-ray images were used to investigate the interface of Li/LSPS further, showing void growth and reduction at 1–4 mA cm^{-2} current density range. Another x-ray-based technique, energy-dispersive x-ray diffraction (EDXRD), offers chemical information of LiMSSBs. *Operando* EDXRD was used to investigate the structural stabilities of $Li_{6.6}Ge_{0.6}Sb_{0.4}S_5I$ and FeS_2,[52] where cathode composite consisted of FeS_2/$Li_{6.6}Ge_{0.6}Sb_{0.4}S_5I$/Carbon additive paired with Li-In as anode. The diffraction contour plot of the full cell is shown in Figure 5b top right, showing the preferred orientation of the large crystallites of $Li_{6.6}Ge_{0.6}Sb_{0.4}S_5I$. EDXRD was interpreted both by spatial position and by time, for instance, the (220) reflection of $Li_{6.6}Ge_{0.6}Sb_{0.4}S_5I$ was compared in intensity from different positions (Figure 5b, bottom left) and peak shift as a function of time (Figure 5b, bottom right).

In solid-state cell setup, especially in the LiMSSB, the stack pressure of the cell is a crucial parameter to control.[53] However, one thing we need to consider is controlling the cycling pressure of the LiMSSB because the volume expansion of lithium metal is severe as it is plated as lithium metal. Therefore, *operando* electrochemical pressiometry gives us a reasonable insight into how to control the actual cycling pressure of the full cell. The recent study relating the critical density of the LiMSSB to cell pressure change during cycling demonstrated that the higher cycling pressure would induce the early cell shorting; therefore, the cell cycling pressure should be actively controlled to minimize the cycling pressure change.[27] In Figure 5c, The cell with springs to maintain constant cycling pressure showed only 0.2 MPa pressure change whereas the fixed gap cell suffered 2 MPa of pressure change.

Practical-level (centimeter-level) characterization

Monitoring the battery during operation is a high-demand technique because it is directly correlated to the safety of the battery. In the practical-level cells, the volume change and

contact loss would become more severe because they operate for much higher capacity than the laboratory-scale cells. Unlike liquid electrolytes acting as buffers even after the volume change, LiMSSBs rely on solid–solid contact, which leads to contact loss and higher local current density. Therefore, further understanding of the true chemo-mechanical properties of solid-state batteries is crucial, where traditional battery management systems' voltage, current, and pack temperature information could not deliver. Note that the literature discussed in the practical-level section is all from liquid-electrolyte-based studies since the majority of LiMSSB studies so far are limited to the laboratory-scale level. However, considering recent industrial efforts to make SSBs the next-generation batteries, a practical-level analysis is needed to evaluate the validity of SSBs in the market. The previous practical-level characterization of liquid-electrolyte-based studies, including optical fiber sensors, x-ray computed tomography, and ultrasonic reflection technique could all be potentially applicable to investigate LiMSSBs in future. Thus, the following section will cover each technique and which properties batteries were evaluated using these tools.

The optical fiber Bragg grating (FBG) sensors are more advanced sensing technology in a way that they could be used to probe heat and stress evolution inside the batteries. The working mechanism of optical fiber is that the photo-induced FBG sensor acts as a reflector for a specific wavelength (Bragg wavelength, $\lambda_B = 2n_{eff}\Lambda$, where n_{eff} is the effective refractive index of the fiber core and Λ is the period of the interference pattern creating the grating). Any changes in temperature (T), pressure (P), and strain to the FBG sensor result in the shift of Bragg wavelength, induced by the change in n_{eff} or Λ.[54] In fact, the study of *operando* temperature monitoring 18,650 cells compared the implanted FBG and thermocouple's response as the cell cycle.[55] In **Figure** 6a, the temperature difference between FBG measure internal temperature and the thermocouple measure external temperature was shown. At a lower rate of 0.5C (yellow shaded), the temperature difference between the two sensors was almost identical. However, as the cycling rate got higher, the temperature difference between the two sensors became preeminent. Figure 6a shows the clear trend of increased discrepancies from 0.95°C for 1C to 3.71°C for 2C discharge. This result indicates that a FBG sensor would be a more accurate option to assess the temperature change in higher-rate cycling. The FBG sensor could be used to evaluate the stress/strain measurement at the surface and inside the battery. Blanquer et al. performed an extensive study

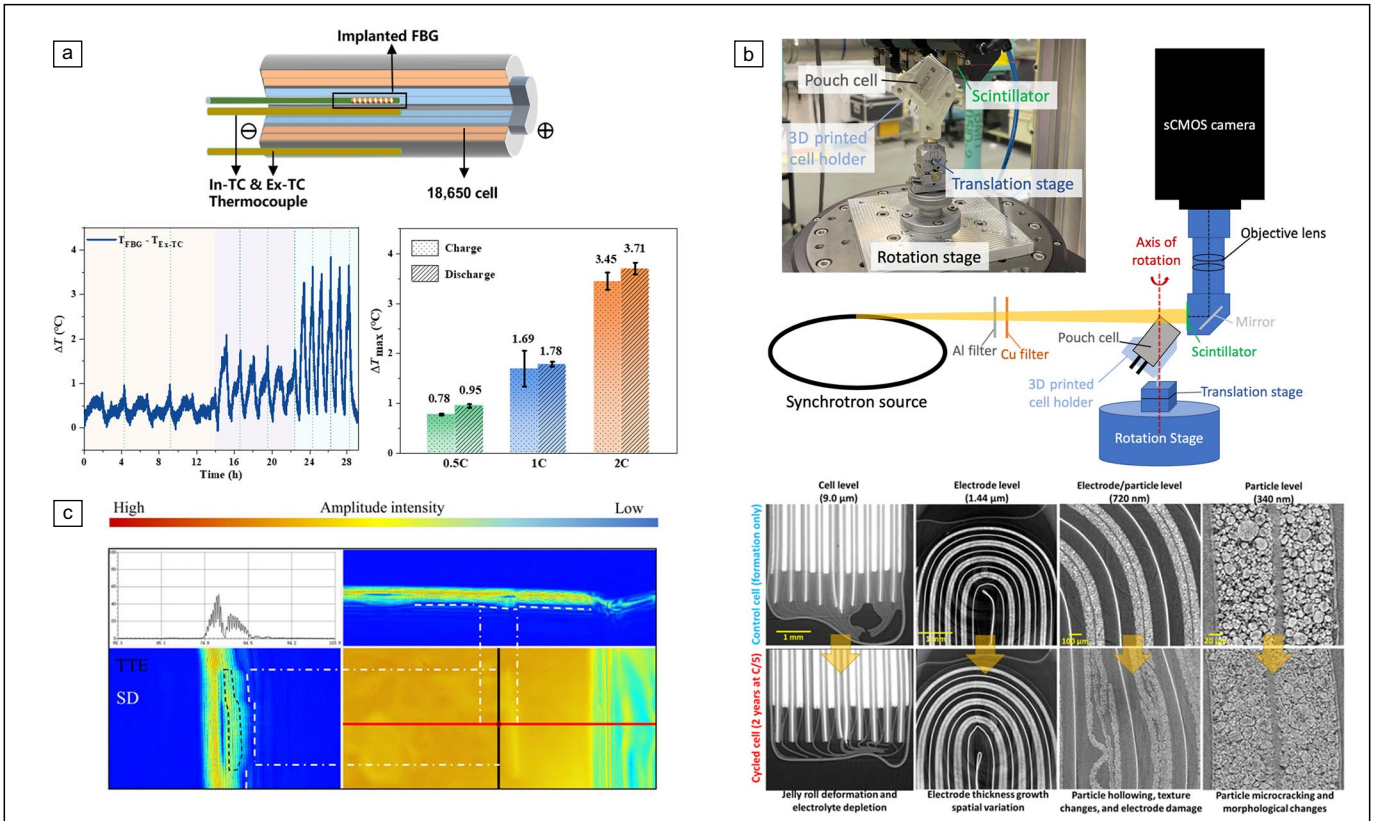

Figure 6. (a) Comparison of the thermocouple and fiber Bragg grating (FBG) measured temperature of the 18,650-cell at different cycling rates. Reprinted with permission from Reference 55. © 2021 Elsevier. (b) The multiscale 3D reconstruction from x-ray computed tomography on a 402,035-size pouch cell. Reprinted with permission from Reference 57. © 2022 The Electrochemical Society. (c) Ultrasonic reflection images of Cu-foil defects at the anode side of the pouch cell. Reprinted with permission from Reference 59. © 2021 Frontiers Media S.A. TC, thermocouple; sCMOS, scientific complementary metal oxide semiconductor; TTE, through transmission enhancement.

on *operando* stress monitoring in both liquid and solid-state electrolytes with the FBG fiber embedded within the $Li_{0.6}In$ electrode, showing the Bragg wavelength shift induced by the cell's stress change.[56]

For characterizing the whole pouch cell, a different length scale measurement tool is needed. The computed tomography mentioned in the previous section is limited to a reduced-size *operando* cell setup to be measured in a synchrotron setup. The synchrotron setup with high photon flux and monochromatic beam energy profile enables the nanometer-scale resolution and segmentation; however, it is far from applicable to investigate the real-scale pouch cell because it requires miniaturized cell setup. The laboratory-scale computed tomography (CT) has the advantage of still being able to deliver high spatial resolution with a reasonable sample stage size. The study performed micro-CT on 402,035-size pouch cells and demonstrated the full multiscale imaging capability (Figure 6b).[57] The scale of the scan varied from the full-cell level scan with 9-µm resolution to the particle-level scan with a resolution of 340 nm. This research highlights how powerful CT could be in the battery field to investigate micro-to-cell-level phenomena.

Another tool to characterize the practical cells in a nondestructive way is to utilize the ultrasonic instrument. Due to the high sensitivity to mechanical properties and porosity of materials, ultrasonic technology has been adopted to investigate the state of charge,[58] metal defect detection,[59] and wetting[60] of the batteries. Yi et al.[59] demonstrated the capability of ultrasonic tomography to detect a defect of metal inside the pouch cell where the change in amplitude of the sound wave is the indicator for the presence of the defect. In Figure 6c, the point where amplitude intensity dropped, the blue regime in the middle of the pouch, is the Cu defect point. Beyond this defect, the sound wave gained back the amplitude (black dotted area) and passed across the rest of the pouch, indicating the defect did not absorb the sound waves.

Conclusion

Realizing high-energy-dense solid-state batteries is one of the most pressing environmental and technological challenges posed to the energy-storage community. Solving the major issues currently known will ultimately demand perspectives from various disciplines and skill sets. This comprehensive article has shed light on the critical analysis of LiMSSBs, with a particular focus on the challenges and opportunities arising from interface-, cell-, and practical-level components. As we strive to unlock the full potential of these advanced energy-storage systems, it becomes evident that collaborative efforts for overcoming the obstacles within the materials community are essential for driving innovation and progress.

1. The interfaces in LiMSSBs have been identified as key elements influencing the overall performance and stability of the system. Throughout this article, we have explored how these interfaces introduce new challenges, such as dendrite formation, interfacial resistance, and limited ion diffusion, and how we analyze those challenges for pursuing commercial-level consideration. By leveraging interdisciplinary approaches and fostering collaboration, we can devise innovative solutions to manipulate and engineer the interfaces, paving the way for enhanced performance and safety of LiMSSBs.
2. From an industry perspective, it is imperative to emphasize the implementation of nondestructive and postmodern advanced testing and analyzing methods to ensure the integrity and reliability of LiMSSBs. By adopting methodologies introduced in this article, industry professionals can gain valuable insights into the internal structure and performance of batteries.
3. To accelerate learning and progress in the field of LiMSSBs, building comprehensive databases and promoting correlative characterization approaches are paramount. A centralized database that consolidates data from various researchers will serve as a valuable resource. Furthermore, adopting correlative characterization techniques that combine multiple analytical methods will yield a more in-depth understanding of several levels of issues and, thus, the impact on battery performance. This integrative approach will provide a more accurate representation of complex interfacial phenomena and accelerate the development of innovative materials and designs.

The analysis of LiMSSBs presented in this article emphasizes the need for collaborative efforts. By collectively addressing the challenges posed by various scale issues, including materials, electrodes, cells, and large-scale systems, we can propel the advancement of LiMSSBs and revolutionize energy-storage technologies. Together, we embark on a journey of discovery and innovation, shaping a sustainable future for energy storage that holds great promise for global sustainability and prosperity.

Acknowledgments

This work by J.J. was supported by the Sogang University Research Grant of 2023 ('202310026.01'). This work was funded by the LG Energy Solution through the Frontier Research Laboratory (FRL) program.

Author contributions

S.-Y.H. contributed to conceptualization, investigation, visualization, validation, and writing-original draft. A.C. contributed to conceptualization, investigation, visualization, validation, and writing-original draft. Y.S.M. contributed to supervision, writing-review and editing, and project administration. J.J. contributed to conceptualization, supervision, writing-review and editing, and project administration.

Funding

Not applicable.

Data availability

Not applicable.

Conflict of interest

On behalf of all authors, the corresponding author states that there is no conflict of interest.

References

1. X. Liu, F. Zhao, J. Geng, H. Hao, Z. Liu, *iScience* **26**, 106654 (2023)
2. J. Asenbauer, T. Eisenmann, M. Kuenzel, A. Kazzazi, Z. Chen, D. Bresser, Sustain. *Energy Fuels* **4**, 5387 (2020)
3. Z. Chang, H. Yang, X. Zhu, P. He, H. Zhou, *Nat. Commun.* **13**, 1510 (2022)
4. Q. Zhao, S. Stalin, C.-Z. Zhao, L.A. Archer, *Nat. Rev. Mater.* **5**, 229 (2020)
5. L. Han, L. Wang, Z. Chen, Y. Kan, Y. Hu, H. Zhang, X. He, *Adv. Funct. Mater.* **33**(32), 2300892 (2023). https://doi.org/10.1002/adfm.202300892
6. Y. Guo, S. Wu, Y.-B. He, F. Kang, L. Chen, H. Li, Q.-H. Yang, *eScience* **2**, 138 (2022)
7. L. Meabe, I. Aldalur, S. Lindberg, M. Arrese-Igor, M. Armand, M. Martinez-Ibañez, H. Zhang, *Mater. Futures* **6**, 1755 (2023)
8. D.H.S. Tan, Y.S. Meng, J. Jang, *Joule* **6**, 1755 (2022)
9. L. He, Q. Sun, L. Lu, S. Adams, *ACS Appl. Mater. Interfaces* **13**, 34320 (2021)
10. H.G. Lee, S.Y. Kim, J.S. Lee, *NPJ Comput. Mater.* **8**, 103 (2022)
11. S. Wang, H. Xu, W. Li, A. Dolocan, A. Manthiram, *J. Am. Chem. Soc.* **140**, 250 (2018)
12. W.D. Richards, L.J. Miara, Y. Wang, J.C. Kim, G. Ceder, *Chem. Mater.* **28**, 266 (2016)
13. D.H.S. Tan, A. Banerjee, Z. Chen, Y.S. Meng, *Nat. Nanotechnol.* **15**, 170 (2020)
14. A. Banerjee, X. Wang, C. Fang, E.A. Wu, Y.S. Meng, *Chem. Rev.* **120**, 6878 (2020)
15. N. Kamaya, K. Homma, Y. Yamakawa, M. Hirayama, R. Kanno, M. Yonemura, T. Kamiyama, Y. Kato, S. Hama, K. Kawamoto, A. Mitsui, *Nat. Mater.* **10**, 682 (2011)
16. Y. Seino, T. Ota, K. Takada, A. Hayashi, M. Tatsumisago, *Energy Environ. Sci.* **7**, 627 (2014)
17. D.H.S. Tan, E.A. Wu, H. Nguyen, Z. Chen, M.A.T. Marple, J.-M. Doux, X. Wang, H. Yang, A. Banerjee, Y.S. Meng, *ACS Energy Lett.* **4**, 2418 (2019)
18. E.A. Wu, C. Jo, D.H.S. Tan, M. Zhang, J.-M. Doux, Y.-T. Chen, G. Deysher, Y.S. Meng, *J. Electrochem. Soc.* **167**, 130516 (2020)
19. F. Walther, F. Strauss, X. Wu, B. Mogwitz, J. Hertle, J. Sann, M. Rohnke, T. Brezesinski, J. Janek, *Chem. Mater.* **33**, 2110 (2021)
20. Y. Liang, H. Liu, G. Wang, C. Wang, Y. Ni, C. Nan, L. Fan, *InfoMat* **4**, e12292 (2022)
21. T. Asano, A. Sakai, S. Ouchi, M. Sakaida, A. Miyazaki, S. Hasegawa, *Adv. Mater.* **30**, 1803075 (2018)
22. K.-H. Park, K. Kaup, A. Assoud, Q. Zhang, X. Wu, L.F. Nazar, *ACS Energy Lett.* **5**, 533 (2020)
23. C. Wang, K. Fu, S.P. Kammampata, D.W. McOwen, A.J. Samson, L. Zhang, G.T. Hitz, A.M. Nolan, E.D. Wachsman, Y. Mo, V. Thangadurai, L. Hu, *Chem. Rev.* **120**, 4257 (2020)
24. A. Masias, N. Felten, R. Garcia-Mendez, J. Wolfenstine, J. Sakamoto, *J. Mater. Sci.* **54**, 2585 (2019)
25. S. Ding, L. Fairgrieve-Park, O. Sendetskyi, M.D. Fleischauer, *J. Power Sources* **488**, 229404 (2021)
26. X. Zhang, Q.J. Wang, K.L. Harrison, S.A. Roberts, S.J. Harris, *Cell Rep. Phys. Sci.* **1**, 100012 (2020)
27. S.-Y. Ham, H. Yang, O. Nunez-cuacuas, D.H.S. Tan, Y.-T. Chen, G. Deysher, A. Cronk, P. Ridley, J.-M. Doux, E.A. Wu, J. Jang, Y.S. Meng, *Energy Storage Mater.* **55**, 455 (2023)
28. L. Zhang, T. Yang, C. Du, Q. Liu, Y. Tang, J. Zhao, B. Wang, T. Chen, Y. Sun, P. Jia, H. Li, L. Geng, J. Chen, H. Ye, Z. Wang, Y. Li, H. Sun, X. Li, Q. Dai, Y. Tang, Q. Peng, T. Shen, S. Zhang, T. Zhu, J. Huang, *Nat. Nanotechnol.* **15**, 94 (2020)
29. S. Kalnaus, N.J. Dudney, A.S. Westover, E. Herbert, S. Hackney, *Science* **381**, eabg5998 (2023)
30. S. Sarkar, V. Thangadurai, *ACS Energy Lett.* **7**, 1492 (2022)
31. H. Yan, K. Tantratian, K. Ellwood, E.T. Harrison, M. Nichols, X. Cui, L. Chen, *Adv. Energy Mater.* **12**, 2102283 (2022)
32. T.K. Schwietert, V.A. Arszelewska, C. Wang, C. Yu, A. Vasileiadis, N.J.J. De Klerk, J. Hageman, T. Hupfer, I. Kerkamm, Y. Xu, E. Van Der Maas, E.M. Kelder, S. Ganapathy, M. Wagemaker, *Nat. Mater.* **19**, 428 (2020)
33. F. Han, Y. Zhu, X. He, Y. Mo, C. Wang, *Adv. Energy Mater.* **6**, 1501590 (2016)
34. A. Cronk, Y.-T. Chen, G. Deysher, S.-Y. Ham, H. Yang, P. Ridley, B. Sayahpour, L.H.B. Nguyen, J.A.S. Oh, J. Jang, D.H.S. Tan, Y.S. Meng, *ACS Energy Lett.* **8**, 827 (2023)
35. P. Bron, S. Dehnen, B. Roling, *J. Power Sources* **329**, 530 (2016)
36. T. Krauskopf, H. Hartmann, W.G. Zeier, J. Janek, *ACS Appl. Mater. Interfaces* **11**, 14463 (2019)
37. A.L. Davis, E. Kazyak, D.W. Liao, K.N. Wood, N.P. Dasgupta, *J. Electrochem. Soc.* **168**, 070557 (2021)
38. J. Jang, Y.-T. Chen, G. Deysher, D. Cheng, S.-Y. Ham, A. Cronk, P. Ridley, H. Yang, B. Sayahpour, B. Han, W. Li, W. Yao, E.A. Wu, J.-M. Doux, L.H.B. Nguyen, J.A.S. Oh, D.H.S. Tan, Y.S. Meng, *ACS Energy Lett.* **7**, 2531 (2022)
39. J. Auvergniot, A. Cassel, J.-B. Ledeuil, V. Viallet, V. Seznec, R. Dedryvère, *Chem. Mater.* **29**, 3883 (2017)
40. X. Ke, Y. Wang, G. Ren, C. Yuan, *Energy Storage Mater.* **26**, 313 (2020)
41. K. Hikima, M. Totani, S. Obokata, H. Muto, A. Matsuda, *ACS Appl. Energy Storage Mater.* **5**, 2349 (2022)
42. A. Sakuda, A. Hayashi, M. Tatsumisago, *Sci. Rep.* **3**, 2261 (2013)
43. A. Kato, M. Yamamoto, A. Sakuda, A. Hayashi, M. Tatsumisago, *ACS Appl. Energy Mater.* **1**, 1002 (2018)
44. L.E. Marbella, S. Zekoll, J. Kasemchainan, S.P. Emge, P.G. Bruce, C.P. Grey, *Chem. Mater.* **31**, 2762 (2019)
45. F. Han, A.S. Westover, J. Yue, X. Fan, F. Wang, M. Chi, D.N. Leonard, N.J. Dudney, H. Wang, C. Wang, *Nat. Energy* **4**, 187 (2019)
46. X. Zhong, C.A. Wade, P.J. Withers, X. Zhou, C. Cai, S.J. Haigh, M.G. Burke, *J. Microsc.* **282**, 101 (2021)
47. Y. Lu, C.-Z. Zhao, J.-K. Hu, S. Sun, H. Yuan, Z.-H. Fu, X. Chen, J.-Q. Huang, M. Ouyang, Q. Zhang, *Sci. Adv.* **8**, eadd0510 (2022)
48. D. Cheng, T.A. Wynn, X. Wang, S. Wang, M. Zhang, R. Shimizu, S. Bai, H. Nguyen, C. Fang, M. Kim, W. Li, B. Lu, S.J. Kim, Y.S. Meng, *Joule* **4**, 2484 (2020)
49. J. Scharf, M. Chouchane, D.P. Finegan, B. Lu, C. Redquest, M. Kim, W. Yao, A.A. Franco, D. Gostovic, Z. Liu, M. Riccio, F. Zelenka, J.-M. Doux, Y.S. Meng, *Nat. Nanotechnol.* **17**, 446 (2022)
50. P. Pietsch, V. Wood, *Annu. Rev. Mater. Res.* **47**, 451 (2017)
51. J.A. Lewis, F.J.Q. Cortes, Y. Liu, J.C. Miers, A. Verma, B.S. Vishnugopi, J. Tippens, D. Prakash, T.S. Marchese, S.Y. Han, C. Lee, P.P. Shetty, H.-W. Lee, P. Shevchenko, F. De Carlo, C. Saldana, P.P. Mukherjee, M.T. McDowell, *Nat. Mater.* **20**, 503 (2021)
52. X. Sun, A.M. Stavola, D. Cao, A.M. Bruck, Y. Wang, Y. Zhang, P. Luan, J.W. Gallaway, H. Zhu, *Adv. Energy Mater.* **11**, 2002861 (2021)
53. J. Doux, H. Nguyen, D.H.S. Tan, A. Banerjee, X. Wang, E.A. Wu, C. Jo, H. Yang, Y.S. Meng, *Adv. Energy Mater.* **10**, 1903253 (2020)
54. G. Han, J. Yan, Z. Guo, D. Greenwood, J. Marco, Y. Yu, *Renew. Sustain. Energy Rev.* **150**, 111514 (2021)
55. Y. Liu, Z. Liu, W. Mei, X. Han, P. Liu, C. Wang, X. Xia, K. Li, S. Wang, Q. Wang, T. Guo, *Measurement* **203**, 111961 (2022)
56. L. Albero Blanquer, F. Marchini, J.R. Seitz, N. Daher, F. Bétermier, J. Huang, C. Gervillié, J.-M. Tarascon, *Nat. Commun.* **13**, 1153 (2022)
57. T. Bond, R. Gauthier, S. Gasilov, J.R. Dahn, *J. Electrochem. Soc.* **169**, 080531 (2022)
58. G. Davies, K.W. Knehr, B. Van Tassell, T. Hodson, S. Biswas, A.G. Hsieh, D.A. Steingart, *J. Electrochem. Soc.* **164**, A2746 (2017)
59. M. Yi, F. Jiang, L. Lu, S. Hou, J. Ren, X. Han, L. Huang, *Front. Energy Res.* **9**, 806929 (2021)
60. Z. Deng, Z. Huang, Y. Shen, Y. Huang, H. Ding, A. Luscombe, M. Johnson, J.E. Harlow, R. Gauthier, J.R. Dahn, *Joule* **4**, 2017 (2020) □

So-Yeon Ham is a doctoral candidate in the Materials Science and Engineering Program at the University of California, San Diego. She received her BS and MS degrees in chemical engineering from Konkuk University, South Korea, studying the atomic layer deposition of Al_2O_3. Her current research focuses on enabling high-capacity anode materials such as Li metal or Si for all-solid-state batteries. Ham can be reached by email at soham@ucsd.edu.

Ashley Cronk is a doctoral candidate and National Science Foundation Graduate Research Fellow in the Materials Science and Engineering program at the University of California, San Diego. She received her BS degree in civil and environmental engineering from the University of California, Berkeley, where she researched and developed electrode-catalyst architectures for (photo)electrochemical reduction of carbon dioxide. Her current research focuses on overcoming interfacial challenges of low-cost sustainable cathode materials (i.e., $LiFePO_4$ and Li–S) for high-energy-dense all-solid-state batteries. Cronk can be reached by email at acronk@ucsd.edu.

Ying Shirley Meng is a professor of Molecular Engineering at the Pritzker School of Molecular Engineering at The University of Chicago and is an adjunct professor at the University of California, San Diego, since 2021. She serves as the chief scientist for the Argonne Collaborative Center for Energy Storage Science (ACCESS) at Argonne National Laboratory. Her research focuses primarily on energy-storage materials and systems—including rechargeable batteries for electric vehicles and trucks, power sources for the Internet of Things, as well as grid-scale storage for deep renewable energy penetration. She has led the development of liquefied gas electrolytes, allowing for a new class of battery that can operate at –112°F; the technology led to the startup South 8 Technologies. Meng can be reached by email at shirleymeng@uchicago.edu.

Jihyun Jang is an assistant professor at Sogang University, South Korea. He received his BS and PhD degrees from the School of Chemical and Biological Engineering at Seoul National University, South Korea. During his studies, he focused on researching transition-metal oxide anode materials for lithium-ion batteries. He subsequently worked at the Samsung Advanced Institute of Technology and Samsung SDI, where he developed lithium-ion batteries suitable for high-energy–density electric vehicles. As a postdoctoral researcher at the University of California, San Diego, he concentrated on the development of materials and systems for all-solid-state batteries. His current research focuses on rechargeable battery systems utilizing electrochemistry and analytical chemistry. Jang can be reached by email at jihyunjang@sogang.ac.kr.